

Research Article

Dynamic Performance Improvement Using Model Reference Adaptive Control of Photovoltaic Systems under Fast-Changing Atmospheric Conditions

Yves Abessolo Mindzie ¹, Joseph Kenfack,¹ Voufo Joseph,¹ Urbain Nzotcha,¹ Dieudonné Marcel Djanssou,² and Raphael Mbounguen¹

¹Laboratory of Energy, Water and Environment, National Advanced School of Engineering of Yaounde, University of Yaounde1, Cameroon

²Department of Renewable Energy, National Advanced School of Engineering of Maroua, University of Maroua, Cameroon

Correspondence should be addressed to Yves Abessolo Mindzie; abessoloyves10@gmail.com

Received 14 July 2022; Revised 18 November 2022; Accepted 25 July 2023; Published 29 August 2023

Academic Editor: Francesco Riganti-Fulginei

Copyright © 2023 Yves Abessolo Mindzie et al. This is an open access article distributed under the Creative Commons Attribution License, which permits unrestricted use, distribution, and reproduction in any medium, provided the original work is properly cited.

The effectiveness of a photovoltaic (PV) system can be increased by using maximum power point tracking (MPPT). The literature has suggested a number of methods for tracking the maximum power point (MPP). However, this number of methods most often presents a high convergence speed in reaching the MPP, complexity under their implementation, power fluctuations, overshoots, and great difficulty in reaching the MPP under fast-changing atmospheric conditions, thus influencing the efficiency of PV systems. Intending to improve the performance of PV systems under rapid changes in the atmosphere, this paper proposes model reference adaptive control (MRAC) as a technique for tracking the MPP based on the employ of reference models such as optimal voltage and current at the MPP (V_{MPP} and I_{MPP}). The MATLAB/Simulink environment is used to produce the simulation results; the Kyocera Solar KC 130 GT module is used here as a photovoltaic power plant, connected to a boost converter, supplying a resistive load. The Lyapunov theory was used to demonstrate the stability of the system. The simulation outcomes obtained using the suggested method are compared with those obtained by techniques such as perturb and observe (P&O), incremental conductance (INC), variable step incremental conductance (VSINC), particle swarm optimization (PSO), and grey wolf optimization (GWO), thus showing a very large improvement under standard test and fast-changing atmospheric conditions of the technique proposed on the other techniques in terms of convergence speed and tracking efficiency. The simulation results prove that the suggested method has great tracking effectiveness (>99.88%), less time for convergence (<0.01 s), and simple implementation complexity under fast-changing atmospheric conditions without both transient and steady-state power oscillations, overshoots, and chattering effects, thus causing a great minimization of energy losses, and the proposed technique reaches exactly the MPP under fast-changing atmospheric conditions.

1. Introduction

Due to the increasing concern over energy use in recent years, the rapid rise in demand is related to industrialization and population development [1]. In spite of this rising demand, no amount of energy available can be sufficient, and the use of fossil fuels is declining [2]. In addition, the diminishing supply of fossil fuels, the rise in oil cost, and the environmental issues with traditional energy sources,

such as global warming [3], we turn to alternative energy sources because of the effects of carbon emissions from the burning of fossil fuels and environmental contamination [4]. Recently, the energy produced from clean, efficient, and nonharmful sources vis-à-vis the environment has become one of the main energy sources of the biggest difficulties faced by scientists and engineers [5, 6]. Considering all the sources of renewable energy, solar-powered power systems are one of these sources that are attracting more

attention because they offer excellent opportunities for the power generator. However, we note that PV systems are strongly nonlinear owing to changes in temperature and irradiance, thus affecting the efficiency of PV systems.

Although many studies have been done to improve the effectiveness of solar-powered cells [7–9], by adjusting the DC-DC converter's duty cycle located between the PVG and load, a perfect flow of electricity from the PVG to the load can be achieved. Having the most solar power possible, photovoltaic (PV) systems are required to operate at the maximum power point (MPP) under different weather conditions and partial shading conditions (PSC), further to an electronic power converter [10]. With both benefits and drawbacks, maximum power point tracking (MPPT) is therefore the most practical and affordable method to enhance the overall efficiency of the PV system [11–14]. The primary goal of the MPPT controller is to maximize the power output from solar panels regardless of the weather [15]. The measured voltage and current of the PV array are commonly used by these MPPT algorithms; the power is calculated, and the duty cycle of the inverter is adjusted to track MPP. Despite having similar goals, the control variable level of complexity, application cost, oscillations around the MPP, and convergence speed approaches vary. However, the photovoltaic array's output power is influenced by meteorological factors including temperature and solar irradiation [11, 12, 16].

Over the past two decades, a number of standard MPPT algorithms have been discussed in the literature, including hill climbing [17] and the fractional short circuit current method [18]. This strategy is comparable to the MPPT but has some disadvantages such as the short-circuit current. That is, 85–95% of an optimum current, so it is not linear, and a loss of energy occurs by the Joule effect during the time of short circuit required for the measurement of the reference. The fractional open-circuit voltage method [19] has some disadvantages as well and does not take into account the characteristics of the photovoltaic module. In addition, the optimum voltage is 75–95% of the open-circuit voltage. Perturb and observe (P&O) [20–22], the disadvantages of the P&O MPPT approach include convergence speed, the explanation of the direction of the disturbance, and oscillations near the MPP [23]. In the goal to overcome these drawbacks, in the literature, perturbation size adaptive methods have been presented [24, 25]. The incremental conductance (INC) approach [26], which is based on a derivative of the output power of a PV panel as a function of its voltage, has been discovered to be more effective. The INC technique offers numerous benefits over the P&O technique by way of tracking speed, tracking precision, and effectiveness. On the other hand, the INC MPPT technique is more difficult, and in real-world applications, noise and inaccuracies in the measured control values have a negative impact on the algorithm's performance [27, 28], model predictive control [29], and synergistic nonlinear fractional control [30]. However, the best algorithms are P&O and INC because they present many advantages such as reduced implementation costs and fewer parameter measurements. Yet, these algorithms are unable to find the MPP under

fast-changing environmental conditions. These methods use a local search space to look for the maximum power point (MPP) [15, 24]. These approaches are only a single peak on the power against voltage (P-V) curve, which represents the output of the PV array [31, 32] because they are restricted to a very small region [15, 24]. Under partially shaded or other nonuniform insolation conditions, multiple peaks may appear across the whole P-V curve [33]. Due to the operation of the bypass diode, MPPT approaches, such as those previously described that are limited to local search for the MPP, can only identify a peak rather than the global peak that symbolizes the global maximum power point (GMPP) [10] on the shaded (silicon) modules [10, 34, 35]. Moreover, these conventional techniques suffer from a quick computation processor, which is necessary for real-time derivative calculation.

The literature proposes adjustments to the traditional MPPT to address the aforementioned issue such as learning-based perturb and observe (LPO) [36], self-turned perturb and observe [37], variable step incremental conductance (VSINC) [38, 39], learning-based incremental conductance (LIC) [40, 41], learning-based hill climbing (L-HC) [42, 43], modified butterfly [44], and improved differential evolution [45]. Global maximum power point tracking in dynamic atmospheric circumstances or in partial shading conditions, in the literature, intelligent MPPT approaches have been proposed with the aim of also correcting the standard MPPT approaches in terms of precision, complexity, etc. These intelligent MPPT approaches are based on metaheuristic optimization methods [46, 47] such as particle swarm optimization (PSO) [48], grey wolf optimization (GWO) [49], cuckoo search (CS) [50], fireflies [51], Jaya algorithm (JA) [52], differential evolution (DE) [53], squirrel search algorithm (SSA) [54], genetic algorithm (GA) [55], artificial bee colony (ABC) [56], neural networks (ANN) [57], and fuzzy logic controller (FLC) [58]. These metaheuristic MPPT techniques are chosen according to performance parameters such as precision, effectiveness, tracking speed, implementation cost, complexity, and flexibility [46]. To determine the maximized power solution subject to PSC, the decision variables voltage, duty cycle, and current are used as the population of particles (candidate solutions); when maximizing an objective function, the PV output power is used. These MPPT approaches have some drawbacks, such as longer settling times and power oscillations. These MPPT approaches are generally precise and stable in stable situations, but less accurate in unstable conditions. These metaheuristic algorithms perform worse than the traditional ones in terms of tracking speed [59]. Transient oscillation of the system's output voltage is a common issue with MPPT algorithms. These metaheuristic MPPT techniques also suffer from tracking the MPP in rapidly changing atmospheric conditions because the electrical parameters become uncertain and variable. In conclusion, these methods vary in a number of areas, including ease of use, speed of convergence, price, and efficacy.

Because of the imperfections that show metaheuristic algorithms, the cheap MPPT control algorithm would be less expensive, simpler, and capable of achieving a speedy

converge to the MPP with minimal oscillation, overshoots, and chattering effects. The MRAC, based on the employ of a model called “reference model” that governs the desired behavior of the system, has been designed to control systems that have unknown parameters; in control domains like robotics and motor control, uncertain or variable parameters have been accepted to combat some parametric fluctuations as well as unidentified internal and external disturbances [60]. A principle of MRAC is therefore to converge the system to be controlled towards the reference model by adjusting the controller parameters according to tracking error while making this error tend towards zero. The simplicity and adaptability of the MRAC approach allow it to be programmed to account for the power system’s inherent nonlinearities with digital converters. Compared to traditional control methods, the fast dynamic reaction and strong stability margin provided by MRAC make it an excellent choice for PV systems working under dynamic environmental conditions. Recently, a few studies with an emphasis on the MPPT for PV systems have been published by the MRAC algorithm [61]. The presented work by Raghav et al. [61] develops a two-level adaptive control design that can handle environmental changes and photovoltaic system uncertainties while also reducing system complexity. Ripple correlation control (RCC) is the initial level of regulation, and model reference adaptive control (MRAC) is the next stage. The inputs to the RCC unit at the first control level are the array voltage V_{PV} and power P_{PV} . The RCC unit then determines the duty cycle $d(t)$ of the system to supply the load in the steady state with the maximum available power. The second control level improves the dynamics of the complete photovoltaic power conversion system or plant to get rid of any potential transient oscillations in the system’s output voltage using the new duty cycle derived from the RCC unit and is modified to eliminate any potential transient oscillations in the system’s output voltage. After the duty cycle has been changed to take into account quickly changing external circumstances, transient oscillations in the system’s output voltage may occur. The system achieves MPPT with overall system stability by decoupling these two control methods. In earlier research done by Raghav et al., we also observed that using the approach suggested in this study, an action reaction of the output PV voltage contains oscillatory and overshoot transients that vanish slowly and cause power losses that reduce the efficiency of the solar power system. We also observe in the research done by Raghav et al. that the system can converge to the maximum power point in 1 ms thanks to the proposed control algorithm. However, concerning the strategy described in this research, the MRAC technique is immediately utilized in tracking MPP. In contrast to the earlier research, the suggested method has the goal of using the optimal voltage and optimal current of the PVG at MPP as reference models of the system, so as to bring the photovoltaic generator to continually work at its optimal voltage; respectively, its optimal current performance tends an error between the PV voltage and the optimal voltage of the photovoltaic generator and an error between the PV current and an optimal current at MPP toward zero by adjusting the parameters of the MRAC

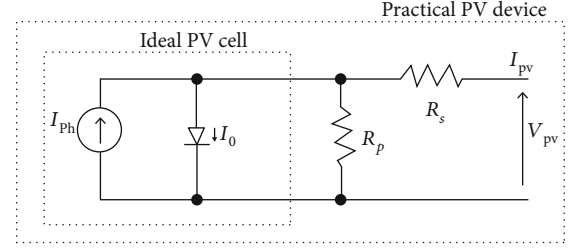


FIGURE 1: Simplified model of a solar-powered cell [62].

controller in both standard and fast-changing atmospheric conditions. This will bring the PVG to continually operate at its optimal power, will minimize power losses, and will improve the PV system’s effectiveness under fast-changing atmospheric conditions. Hence, the suggested MPPT technique has great control effectiveness, quick dynamic response, and accuracy in reaching the MPP without both transient and steady-state oscillations, overshoot, or chattering effects under fast-changing atmospheric conditions.

The remaining parts of the paper are arranged as follows: the model of the photovoltaic system is described in the second half; the third part presents the proposed algorithm; the fourth part titled discussion and simulation results presents the photovoltaic system’s simulation and the results obtained by simulation of the proposer algorithm compared with the results of the conventional algorithms P&O, INC, VSINC, PSO, and GWO and presents the discussion; the fifth part is going to conclude our research work discussed in the paper and bring out the perspectives.

2. Materials and Methods

2.1. Model of Photovoltaic Array. More advanced models that are more accurate and can be used for a variety of applications have been proposed by certain writers. The fundamental equation from the theory of semiconductors, Equation (1), represents the single-diode model shown in Figure 1 by quantitatively describing the I–V characteristics of the PV array [62–64]. The photocurrent (I_{ph}), diode, and shunt resistor (R_p), which represent leakage current, and the series resistor (R_s), which expresses an internal resistance to the circulation of the current and models the ohmic loss of the contacts, are seen in Figure 1.

These electrical models model the cell by an ideal current generator; according to the law of nodes, the output current I is provided by

$$\begin{aligned} I &= I_{PV} = I_{ph} - I_d - I_p, \\ I &= I_{PV} = I_{ph} - I_d - \frac{V_{PV} + I_{PV}R_s}{R_p}, \end{aligned} \quad (1)$$

where I_{ph} is the photocurrent which is constant for a given sunshine, I_d is the current flowing via the diode, I_p is the parallel resistor current leak (shunt resistor), and I_s is the diode’s saturation current.

According to Takuya et al., the equation of the current diode of Figure 1 is defined by Equation (2) as follows (Takuya, Matsubara, & Hitoshi, 2018):

$$I_d = I_0 = I_s \left[e^{q(V+IR_s)/nKT} - 1 \right]. \quad (2)$$

In ideal conditions, we have $R_p = \infty$ and $R_s = 0$, thus Equation (1) becomes:

$$I_{PV} = I_{ph} - I_s \left[e^{q(V+IR_s)/nKT} - 1 \right], \quad (3)$$

where q is the basic electrical charge (electron's charge 1.6×10^{-19} C), K is the constant of Boltzmann (1.38×10^{-23}), V is the voltage at the cell's terminals, n is the ideality factor ($1 < n < 3$), and T is the ambient temperature ($^{\circ}\text{K}$).

From the equations of the simplified model, the model with one diode [65], and the model with two diodes [66] of a photovoltaic cell, we can obtain the mathematical model giving the current supplied by a generator of $n = 36$ identical cells, that is:

$$n = n_p \times n_s, \quad (4)$$

where n_s is the number of consecutive (series) cells ($n_s = 36$) and n_p is the number of parallel cells ($n_p = 1$).

The current supplied can be written as follows:

The simplified model is the following:

$$I = I_{ph} - I_d - I_p, \quad (5)$$

The one-diode model is the following:

$$I_g = I_{gph} - I_d - I_{gsh}, \quad (6)$$

The two-diode model is the following:

$$I_g = I_{gph} - I_{d1} - I_{d2} - I_{gsh}, \quad (7)$$

where the current through the diode is $I_d = n_p \times I_d$.

The current through the resistors connected in parallel:

$$I_{gsh} = n_p \times I_{sh}, \quad (8)$$

$$I_d = I_{gsh} - I_{gs} \left[e^{q(V_g + I_g R_{gs})/nKT} - 1 \right], \quad (9)$$

$$I_d = I_{gsh} - I_{gs} \left[e^{q(V_g + I_g R_{gs})/nKT} - 1 \right] - \frac{V_g + I_g R_{gs}}{R_{gs}}, \quad (10)$$

$$I_d = I_{gsh} - I_{gs1} \left[e^{q(V_g + I_g R_{gs})/n_1KT} - 1 \right] - I_{gs2} \left[e^{q(V_g + I_g R_{gs})/n_2KT} - 1 \right] - \frac{V_g + I_g R_{gs}}{R_{gs}}, \quad (11)$$

The voltage across the generator is the following:

$$V_g = n_s \times I_{s1}. \quad (12)$$

Saturation current resulting from the diodes identical to d_1 (saturation current I_{s1} , ideality factor n_1):

$$I_{gs1} = n_s \times V. \quad (13)$$

Saturation current resulting from diodes identical to d_2 (saturation current I_{s2} , ideality factor n_2):

$$I_{gs2} = n_s \times I_{s2}. \quad (14)$$

Practically, the series resistance (R_s) value is extremely tiny; it has a voltage that is very small compared to the voltage across the generator ($V_g + I_g \cdot R_s \approx V_g$). Therefore, the three equations resulting from the three models become:

The simplified model is the following:

$$I_g = I_{gph} - I_{gs} \left[e^{q(V_g)/nKT} - 1 \right]. \quad (15)$$

The one-diode model is the following:

$$I_g = I_{gph} - I_{gs} \left[e^{q(V_g)/nKT} - 1 \right] - \frac{V_g}{R_{gs}}. \quad (16)$$

The two-diode model is the following:

$$I_d = I_{gsh} - I_{gs1} \left[e^{q(V_g)/n_1KT} - 1 \right] - I_{gs2} \left[e^{q(V_g)/n_2KT} - 1 \right] - \frac{V_g}{R_{gs}}. \quad (17)$$

The photovoltaic generator (PVG) will therefore have as its mathematical model [66]

$$I_{pv} = N_p I_{pv} - N_p I_d \left[e^{(qV_{pv}/N_sKT)} - 1 \right]. \quad (18)$$

The inverse saturation current is

$$I_s = I_{rs} \left(\frac{T}{T_r} \right)^3 e^{(E_g q / (KT(1/T_r - 1/T)))} \quad (19)$$

The reverse saturation current at T_r is

$$I_{rs} = \frac{I_{scr}}{e^{(qV_{oc}/N_sKT)} - 1}, \quad (20)$$

$$I_{ph} = [I_{scr} + (K_i(T - T_r))] \frac{E}{1000}. \quad (21)$$

The power of the photovoltaic generator is

$$P_{pv} = V_{pv} \cdot I_{pv} = N_p \cdot I_{ph} \cdot V_{pv} - N_p \cdot I_0 \cdot V_{pv} \left[e^{(qV_{pv}/N_sKT)} - 1 \right]. \quad (22)$$

2.1.1. Simulation of a Solar Panel. For the simulation of the PV panel, we will use Kyocera Solar KC 130 GT as a photovoltaic generator during the simulation to validate our proposed approach and compare it with other MPPT algorithms, and its electrical characteristics are depicted in Table 1.

TABLE 1: Electrical characteristics of a solar panel.

Parameters	Values	Units
Maximum power point (P_{MPP})	130.064	W
MPP's optimal voltage (V_{MPP})	17.6	V
MPP's optimal current (I_{MPP})	07.39	A
Voltage's open circuit (V_{oc})	21.9	V
Current's short circuit (I_{sc})	8.02	A
Open circuit voltage coefficient temperature (T_{oc})	-0.355	%deg.C
Short-circuit current coefficient temperature of the (T_{sc})	0.06	% deg.C
Nominal's temperature (T_n)	25	Deg.C
Nominal's irradiance (G_n)	1000	W/m ²

The solar photovoltaic system's electrical properties are hardly dependent on the sun's exposure and the surrounding temperature, demonstrating the nonlinearity of the solar photovoltaic system. The current in the function of power (I-P) and voltage (I-V) in the function of voltage (P-V) characteristics of the solar photovoltaic system are depicted in Figure 2 [67]. The PV module is developed in MATLAB/Simulink, and the model allows for four distinct irradiation values G (400 W/m², 600 W/m², 800 W/m², and 1000 W/m²) to be used to follow the behavior of the photovoltaic module for four different irradiations with the same temperature of 25°C.

2.2. DC-DC Converter. Another crucial part of the PV system is the DC-DC converter, which is utilized to collect energy from the linked PV array. To guarantee that the PV array generates the most power possible while tracking, the MPPT controller modifies the duty cycle of the DC-DC converter. Isolated and nonisolated DC-DC converters are the two broad categories into which DC-DC converters can be broadly subdivided [68]. Compared to nonisolated converters, the isolated converter has a more sophisticated structural design. As a result, the suggested approach employs a nonisolated converter. There are many different kinds of nonisolated DC-DC converters, including buck, boost, buck-boost, Cuk, and SEPIC converters, and in our situation, we will utilize a boost converter. The DC-DC converter (boost) in Figure 3 enables adaptation between the PV panel and the load in order to get the most power out of the PV panel [69]. In order to supply the most power possible, we modify the equivalent charge resistor seen by the source using the duty cycle [70]. Its typical application is to convert its input voltage and current, respectively, into a higher output voltage and output current, respectively [66].

Deduction of the mathematical model of our booster is [65]:

$$\begin{aligned}
 i_L(t) &= i_i(t) - C_1 \frac{dv_i(t)}{dt}, \\
 i_0(t) &= (1-d)i_L(t) - C_2 \frac{dv_0(t)}{dt}, \\
 V_i(t) &= L \frac{di_L(t)}{dt} + (1-d)V_0(t).
 \end{aligned} \tag{23}$$

We take into account a hypothetical model, disregarding the transistor's switching time and the values of the internal resistors of the inductor and capacitor. Table 2 in summarizes the electrical characteristics of the boost converter [69].

3. Model Reference Adaptive Control Algorithm

To solve servo problem model reference adaptive control (MRAC) was created based on a reference model to designate a desired system performance [71]. This reference model indicates how the system output should ideally respond to a control signal. The MRAC algorithm has interests such as it is simple to implement, has higher stability compared to other classical controllers of nonlinear systems, ensures stability and quality of control for fairly large limitations to the qualities' ability to vary in the solar-powered system, is very accurate, and has a fast execution time [61, 71]. The fundamental tenet of the reference model's adaptive control consists of adapting the controller parameters according to the error between the system and the reference model. The structure of the MRAC algorithm is given in Figure 4.

Adaptive control by the reference model consists of adopting the controller in such a way that the process behaves like the reference model. Its structure is as follows:

- (i) A first ordinary positive closed-loop containing the reference model and the controller parameter adjustment mechanism
- (ii) A second negative closed loop containing the controller and the boost converter

3.1. Mathematical Model of Reference Model. This is the part of the controller that is represented by a mathematical model in order to achieve the required closed-loop behavior system [61]. A theoretical MPP current was intended to be delivered by the reference model, voltage, and power having a crucial damped step response. The reference model or reference voltage and reference current is used to generate the reference trajectory V_{ref} , I_{ref} and is chosen so that it is less than or equal to an optimal voltage and an optimal current of the solar-powered array at a maximum power point ($V_{ref} \leq V_{MPP}$ and $I_{ref} \leq I_{MPP}$). In this paper, the behavior of the reference model is a constant such that

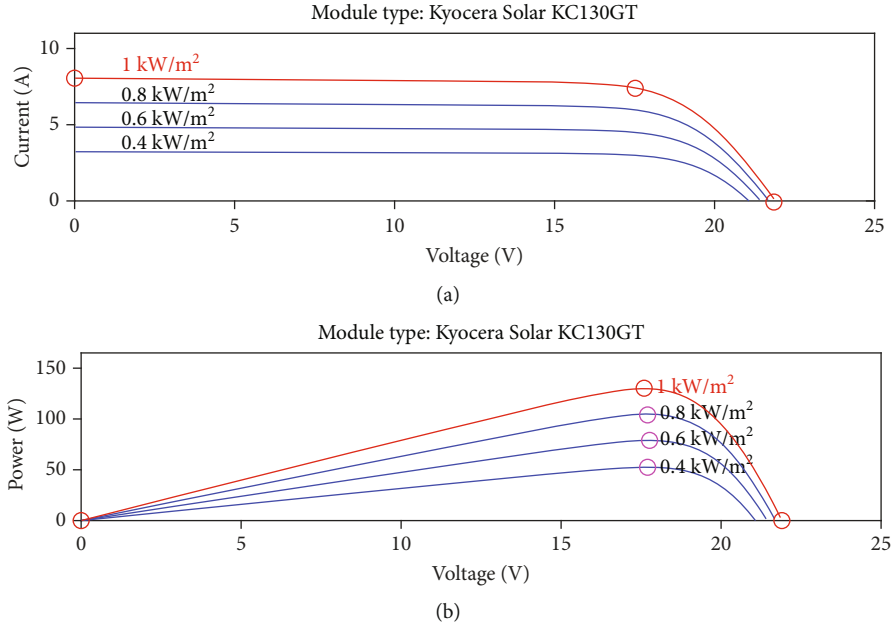


FIGURE 2: (a) I-V and (b) P-V characteristics of the photovoltaic generator with $t = 25^\circ\text{C}$ and irradiation changing.

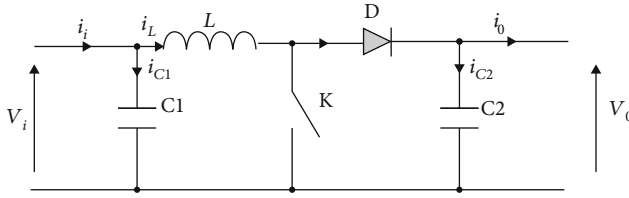


FIGURE 3: The boost converter [66].

TABLE 2: The electrical characteristics of the boost converter [69].

No.	Parameter	Value	Unit
1	Capacitor C_1	100E-6	F
2	Capacitor C_2	12000E-6	F
3	Ripple inductance	0	H
4	Mosfet IGBT: ripple resistor	0.001	Ω
5	Mosfet IGBT: forward voltage	1	V
6	Diode: ripple resistor	0.001	Ω
7	Diode: forward voltage	0.8	V
8	Load resistor	64	Ω
9	Switching frequency	10	Khz

$$\begin{aligned} V_{\text{ref}} &= V_{\text{MPPT}} = 17.6\text{V}, \\ I_{\text{ref}} &= I_{\text{MPPT}} = 07.39\text{A}. \end{aligned} \quad (24)$$

3.2. Adaptive Controller. The adaptive controller has two subparts: the adaptive PID controller (see Figure 5), which has an input error obtained from the difference between the plant's output at the set point, and the adaptation mechanism, which according to the error, adjusted the adaptive PID controller (see Figure 6) [72].

The adaptive PID controller's parameters are deduced by comparing the functional closed-loop transfer with the

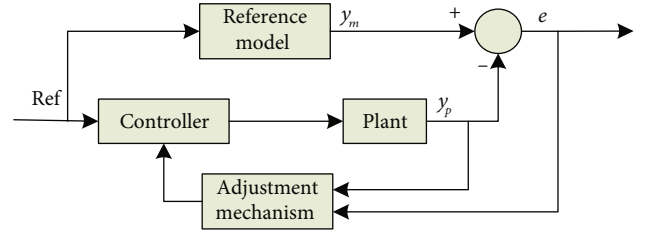


FIGURE 4: Structure of the proposed MRAC algorithm [61].

function's transfer of a system of second-order as follows (see Figure 6):

$$\frac{V_{\text{bus_ref}}}{V_{\text{bus}}} = \frac{K_p \cdot S + K_i/C}{S^2 + K_p/C \cdot S + K_i/C} = \frac{\omega_n^2}{s^2 + 2\delta s + \omega_n^2}. \quad (25)$$

From Equation (25), the controller parameters are shown in Table 3 and determined by the Ziegler-Nichols method [73]

$$\begin{aligned} K_p &= 2 \cdot \delta \cdot \omega_n \cdot C, \\ K_i &= C \cdot \omega_n^2, \\ K_d &= 0, 5 \cdot Tu. \end{aligned} \quad (26)$$

3.2.1. Tracking Errors. The tracking voltage error e_v and tracking current error e_I are defined by $e_v = V_{\text{pv}} - V_{\text{ref}}$ and $e_I = I_{\text{pv}} - I_{\text{ref}}$. The adjustment mechanism is presented in Figure 7 and generates an estimate of the controller parameters $\theta(t)$ [61].

3.3. Photovoltaic System. To offer a real array current, the PV system model was chosen to deliver an actual array, voltage, and power with a step response that is underdamped.

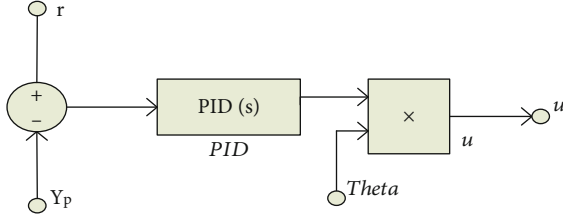


FIGURE 5: Adaptive PID controller [72].

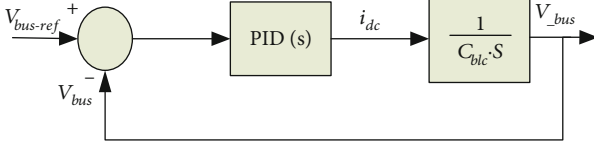


FIGURE 6: Control loop of the DC bus voltage [72].

TABLE 3: The adaptive PID controller's parameters.

Parameters	Values
Kp	4
Ki	100
Kd	0.00005
Mechanism adaptation parameter (gamma)	1
Control parameter voltage (theta1)	1.29
Control parameter current (theta2)	0.93
Control parameter (theta3)	0
Control parameter (theta0)	1

3.3.1. *Controller Architecture.* The architecture controller that allows us to obtain the objective control function is presented in Figure 8 [61].

According to the controller structure in Figure 9, we have

$$u_p = u_0 r + \theta_1 \frac{1}{s + \lambda} u_p + \theta_2 \frac{1}{s + \lambda} y_p + \theta_3 = \theta_0 r + \theta_1 \omega_1 + \theta_2 \omega_2 + \theta_3 y_p = \theta^T \omega, \quad (27)$$

where the vector parameter of the controller

$$\theta = [\theta_0, \theta_1, \theta_2, \theta_3]^T, \quad (28)$$

and

$$\omega = [\theta, \omega_1, \omega_2, y_p]^T, \quad (29)$$

$\omega_1 = (1/s + \lambda)u_p$, $\omega_2 = (1/s + \lambda)y_p$, and $1/s + \lambda$ the stable filter.

$$\begin{aligned} \dot{\omega}_1 &= -\lambda \omega_1 + u_p, \\ \dot{\omega}_2 &= -\lambda \omega_2 + y_p. \end{aligned} \quad (30)$$

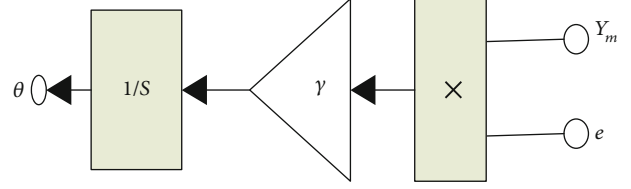


FIGURE 7: Adaptation mechanism [61].

By observing the structure of the controller and the principle of the MRAC algorithm, we will have as a condition the relations $y_p(s)/y_p(s) = y_m(s)/r(s)$ with the new controller setting

$$\theta^* = [\theta_0^*, \theta_1^*, \theta_2^*, \theta_3^*], \quad (31)$$

with $\theta_0^* = k_m/k_p$, $\theta_1^* = a_p - a_m$, $\theta_2^* = (a_p - a_m)(-\lambda^2 - \lambda a_p - b_b)/k_p$, and $\theta_3^* = (b_p - b_m) + (a_p - a_m)(\lambda - a_p)/k_p$.

(1) *The Reference Model and the System's State Models.* Let us consider the set $\{A_p, B_p, C_p\}$, the realization to minimize $Gp(s)$.

$$\begin{aligned} \dot{x}_p &= A_p x_p + B_p u_p, \\ y_p &= C_p x_p, \end{aligned} \quad (32)$$

with x_p dimension 2 (2D) vector.

Considering Equations (29) and (32), the closed-loop system and the controller have an equation of state as follows:

$$\begin{aligned} \dot{x}_{pe} &= A_{pe} x_{pe} + B_{pe} (\theta^T \omega), \\ y_p &= C_{pe} x_{pe}, \end{aligned} \quad (33)$$

with x_{pe} is a defined extended state vector such as $x_{pe} = [x_p^T, \omega_1, \omega_2]^T$

where A_{pe} , B_{pe} , and C_{pe} are matrices defined by

$$A_{pe} = \begin{bmatrix} A_p + \theta_3^* B_p C_p & \theta_1^* B_p & \theta_2^* B_p \\ \theta_3^* C_p & -\lambda + \theta_1 & \theta_2^* \\ C_p & 0 & -\lambda \end{bmatrix}, \quad (34)$$

$$B_{pe} = \begin{bmatrix} B_p \\ 1 \\ 0 \end{bmatrix}, \quad (35)$$

$$C_{pe} = [C_p \quad 0 \quad 0], \quad (36)$$

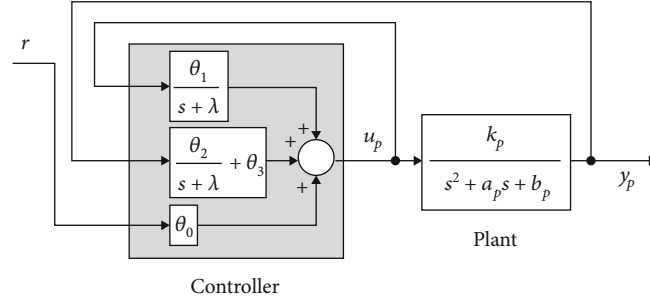


FIGURE 8: Controller architecture [61].

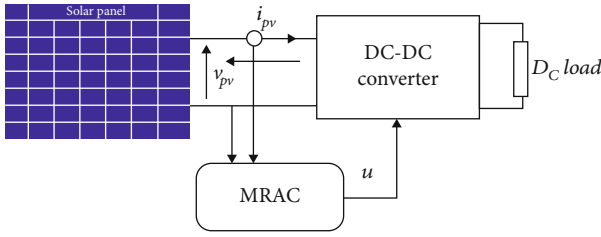


FIGURE 9: Photovoltaic system MRAC MPPT control schematic diagram.

where $u_p = \theta^{*T} \omega$. Then, Equation (36) thus becomes

$$\begin{aligned} \dot{x}_{pe} &= A_{pe} x_{pe} + B_{pe} \theta_0^* r, \\ y_p &= C_{pe} x_{pe}. \end{aligned} \quad (37)$$

Then, the set $\{A_{pe}, B_{pe} \theta_0^*, C_{pe}\}$ allows us to obtain the reference model which will have an equation of state

$$\begin{aligned} \dot{x}_{me} &= A_{pe} x_{me} + B_{pe} \theta_0^* r, \\ y_m &= C_{pe} x_{me}, \end{aligned} \quad (38)$$

where x_{me} is a four-dimensional state vector. A_{pe} can be demonstrated to be asymptotically stable.

3.3.2. Stability Study of the System

(1) *Error Equations.* By differentiating the reference model equations of state with those of the system to be controlled, the state's error equation, the controller error's parameters, and the tracking error are obtained as follows:

$$\begin{aligned} \dot{e} &= A_{pe} + B_{pe} (u_p - \theta^{*T} \omega), \\ e_0 &= C_{pe} e, \end{aligned} \quad (39)$$

where e , e_0 et $\tilde{\theta}$ represents the state error, the tracking error, and the controller error parameter, respectively, according to

$$\begin{aligned} e &= x_{pe} - x_{me}, \\ e_0 &= y_p - y_m, \\ \tilde{\theta} &= \theta - \theta^*. \end{aligned} \quad (40)$$

According to the Lyapunov criteria, the input-output matching law of the transfer function equation of the error state vector must be strictly positive [61, 74]. However, the equation's transfer function (39) is not always strictly positive because

$$C_{pe} (SI - A_{pe})^{-1} B_{pe} = \frac{G_m(s)}{\theta_0^*}. \quad (41)$$

From Equation (40), we obtain Equation (41) which will have two (02) as its relative degree. This two relative degree will imply Equation (41) to be strictly positively defined [75]. To overcome this difficulty, the identity $(s + g)(s + g)^{-1} = 1$ is used for all $g > 0$, and Equation (39) will be written as follows:

$$\begin{aligned} \dot{e} &= A_{pe} + B_{pe} (s + g) (u_g - \theta^{*T}), \\ \dot{e} &= A_{pe} + B_{pe} (s + g) \tilde{\theta}^T \phi, \end{aligned} \quad (42)$$

where $u_g = (1/s + g)u_p$ and $\phi = (1/s + g)\omega$. The sum $s + g$ permits the numerator's degree to increase and the transfer function to become equal to 1. However, $u_g = \theta^{*T} \omega$; the controller's expression can be expressed as follows:

$$\begin{aligned} u_g &= (s + g)u_g, \\ u_g &= \theta^{*T} \phi + \theta^{*T} \omega, \\ u_g &= \dot{\theta}^T \phi + \theta^{*T} (\phi + g), \\ u_g &= \dot{\theta}^T \phi + \theta^{*T} \omega, \\ \bar{e} &= e - B_{pe} \tilde{\theta}^T \phi, \end{aligned} \quad (43)$$

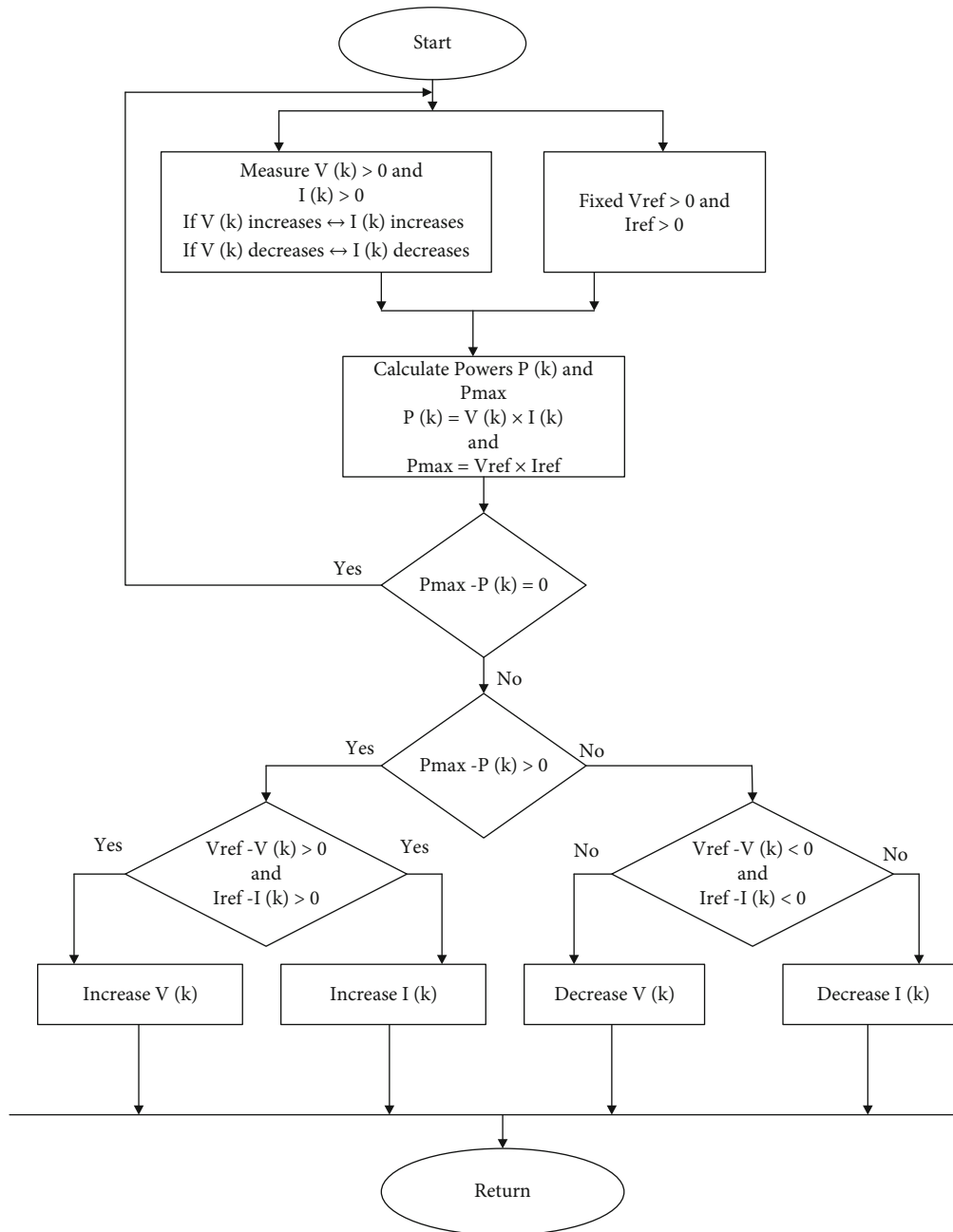


FIGURE 10: The proposed algorithm flow chart.

Its derivative gives

$$\begin{aligned} \dot{\tilde{e}} &= A_{pe}\tilde{e} + \left(A_{pe}B_{pe} + gB_{pe} \right) \tilde{\theta}^T \phi, \\ e_0 &= C_{pe}\tilde{e} + C_{pe}eB_{pe}\tilde{\theta}^T \phi. \end{aligned} \quad (44)$$

Let $B_1 = A_{pe}B_{pe} + gB_{pe}$ and $C_{pe}B_{pe} = 0$ because the reference model's degree is 2, that is, the largest numerator's coefficient $C_{pe}(SIA_{pe})^{-1}B_{pe} = 0$ is equal to 0. Therefore we will have

$$\begin{aligned} \dot{\tilde{e}} &= A_{pe}\tilde{e} + B_1\tilde{\theta}^T \phi, \\ e_0 &= C_{pe}\tilde{e}. \end{aligned} \quad (45)$$

For the new equation's error state (45), its function's transfer from $\tilde{\theta}^T \phi$ to e_0 in (40) by what (41) transformed the equivalent of (43); hence, the set $\{A_{pe}, B_{pe}, C_{pe}\}$ has the following transfer function:

$$(s + g) \frac{Gm}{\theta_0^*} = \frac{Km}{\theta_0^*} \frac{(s + g)}{s^2 + a_m s + b_m}. \quad (46)$$

The positive constant g is chosen such that $g < am$. It is demonstrable that Equation (46) is strictly positive definite for all g such that $0 < g < am$.

(2) *Adaptation Law's Derivation.* Using the adaptation law as a basic, we construct a Lyapunov function having two state vectors: the error controller parameter's $\tilde{\theta}$ and the state's error \bar{e} .

$$V(\tilde{\theta}, \bar{e}) = \frac{\bar{e}^T \bar{P} \bar{e}}{2} + \frac{\tilde{\theta}^T \Gamma^{-1} \tilde{\theta}}{2}, \quad (47)$$

where any positive definite symmetric matrix, Γ , is used and P is an undeniable positive definite symmetric matrix determined by the Lemma of Meyer-Kalman-Yakubovich (MKY) [61, 74]. Since the MKY lemma is stable and A_{pe} is stable and $\{A_{pe}, B_{pe}, C_{pe}\}$ is defined strictly positive in (47), when it comes to a specific definite symmetric positive definite matrix P , a vector q , and a scalar $\nu > 0$ such that

$$\begin{aligned} PA_{pe} + A_{pe}^T P &= -qq^T - V, \\ PB_1 &= C_{pe}^T. \end{aligned} \quad (48)$$

When it comes to all given symmetric positive definite matrix L , matrix P in (47) satisfies (48).

The Lyapunov function's (47) time-derivative together (45) is calculated as:

$$\dot{V} = \left(\tilde{\theta}, \bar{e} \right) = -\frac{1}{2} \bar{e}^T qq^T \bar{e} - \frac{V}{2} \bar{e}^T L \bar{e} + \bar{e}^T PB_1 \tilde{\theta}^T \phi + \tilde{\theta}^T \Gamma^{-1} \dot{\tilde{\theta}}. \quad (49)$$

Since $\bar{e}^T PB_1 \tilde{\theta}^T \phi = \bar{e}^T C_{pe}^T = e_0$, we can choose

$$\dot{\tilde{\theta}} = \tilde{\theta} = -\Gamma e_0 \phi. \quad (50)$$

Thus

$$\dot{V} = \left(\tilde{\theta}, \bar{e} \right) = -\frac{1}{2} \bar{e}^T qq^T \bar{e} - \frac{V}{2} \bar{e}^T L \bar{e} \leq 0. \quad (51)$$

According to the adaptation law (Equation (50)), the condition (Equation (51)) will always be met, which ensures that both the tracking error and the control parameter error are stable and bounded [76]. Using the aforementioned derivations above, the general MRAC rules can be stated as follows:

$$\begin{aligned} \dot{\omega}_1 &= -\lambda \omega_1 + u_p, \\ \dot{\omega}_2 &= -\lambda \omega_2 + y_p, \\ \dot{\phi} &= -\dot{g} \phi + \omega, \\ u_p &= \theta^T + \dot{\theta}^T \phi = \theta^T \omega - \phi^T \Gamma e_0 \phi, \\ \dot{\theta} &= -\Gamma e_0 \phi. \end{aligned} \quad (52)$$

3.3.3. *Photovoltaic System MRAC MPPT Control Schematic Diagram.* Figure 9 shows the photovoltaic system optimization schematic diagram by the proposed MRAC MPPT algorithm with the goal to transfer to the load of an optimal power.

3.3.4. *MRAC MPPT Control Flow Chart.* The proposed algorithm flow chart is presented in Figure 10 showing the implementation method of our proposed algorithm.

4. Simulation Results and Discussion

4.1. *Current and Voltage Tracking of the Proposed Algorithm under Standard Test Conditions before 0.1 Seconds.* To evaluate whether the suggested control algorithm is effective at a reference voltage and current chosen, respectively, such as $V_{ref} = V_{MPPT} = 17.6$ V and $I_{ref} = I_{MPPT} = 07.36$ A, we used as a source the Kyocera Solar KC 130 GT Photovoltaic Generator with a maximum power of $P_{max} = MPP = 130$ W, where these P-V characteristics are tabulated in Table 1. The simulations were done using MATLAB/Simulink software under normal test conditions ($G = 1000$ W/m² and $T = 25^\circ$ C), as shown in Figure 11.

The verification of the maximum current and error current point tracking by the output of the photovoltaic generator so that it works continuously to supply the load with the most power possible using a proposed approach in standard test conditions was done in Figure 12. Figure 12 shows that the error between the reference current and the PV current converges to 0. A theoretical MPP current with a critically damped step response was intended to be delivered by the reference current model.

The voltage and error voltage point tracking in Figure 13 proves that the photovoltaic generator works optimally so that the voltage delivered by the photovoltaic generator perfectly follows the optimal voltage or maximum voltage point (MVP). Figure 13 shows that the error between the reference voltage and the PV voltage converges to 0. A theoretical MPP voltage with a critically damped step response was intended to be delivered by the reference voltage model.

The changes to the controller's parameters of the theta1 (for control of the voltage) and theta2 (for current control) during the simulation test are depicted in Figures 14(a) and 14(b). Figure 14 gives us the maximum duty ratio of 0.7, theta1 max = 1.29, and theta2 max = 0.93 (the parameters converge to the ideal); the obtained values affirm the good tracking of the optimal current and voltage. For a correct operation, the duty ratio has a range between 0 and 0.75.

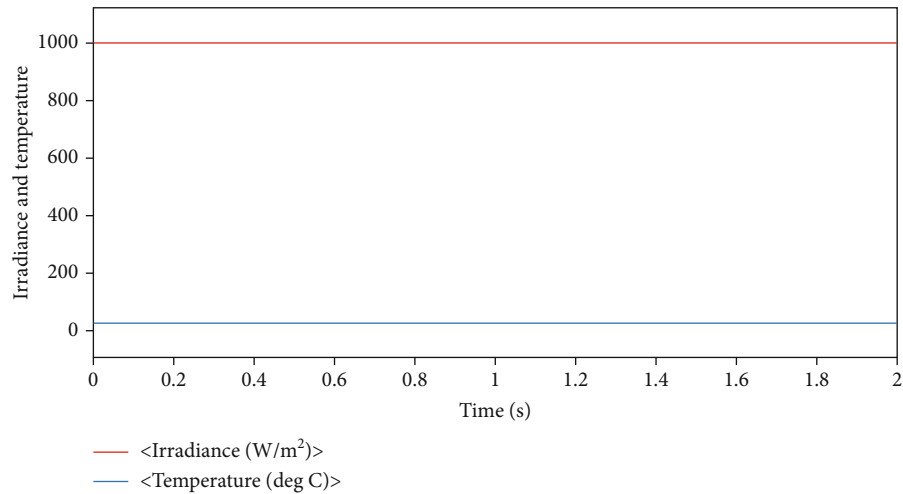


FIGURE 11: Normal test conditions $G = 1000 \text{ W/m}^2$ and $T = 25^\circ\text{C}$.

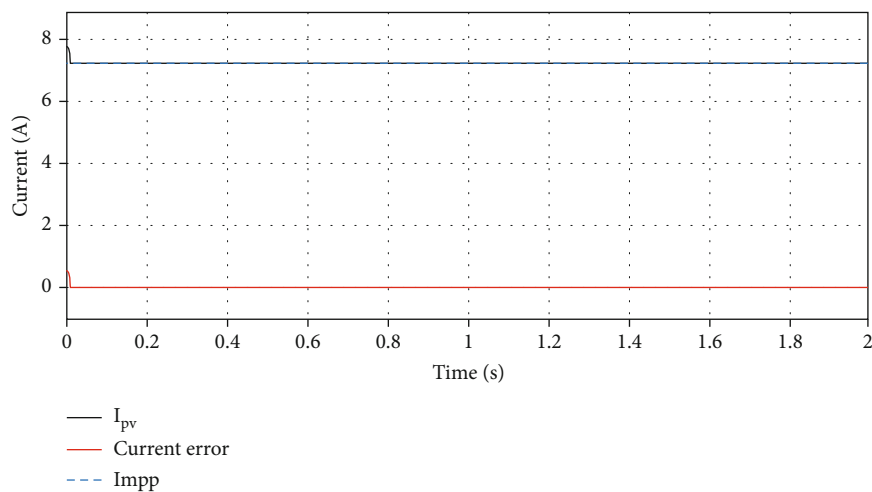


FIGURE 12: MRAC maximum current and error point tracking in standard test conditions.

4.2. *Tracking of the MPPT by Conventional Algorithms and the Proposed Algorithm in Standard Test Conditions before 0.1 Seconds.* Over a sampling time of 0.1 seconds, Figure 15 shows that only the PSO MPPT algorithm is unstable and does not follow a maximum power point (MPP), while the GWO MPPT approach shows slight fluctuations in power around the MPP that are associated with energy losses.

4.3. *Tracking of the MPPT by the Conventional Algorithms and the Proposed Algorithm in Standard Test Conditions before 0.2 Seconds.* Before 0.2 seconds, under standard test conditions, all MPPT control algorithms as shown in Figure 16 follow a maximum power point under a steady-state system. This figure shows that under the standard test conditions, before 0.2 seconds, these different MPPT techniques are stable and accurate.

4.4. *Evaluation of the Robustness of the Conventional and Proposed Algorithms (Fast-Changing of Atmospheric Conditions) before 0.2 Seconds*

4.4.1. *Tracking Current and Voltage by the Proposed Approach under Fast-Changing Atmospheric Conditions before 0.2 Seconds.* With the view to evaluating the robustness of the proposed MPPT approach, according to Figure 17, we switched from normal and stable conditions to fast variations of atmospheric conditions while adjusting the sun irradiance and maintaining the temperature at 25°C .

The good tracking of the global maximum current point (MCP), Figure 18(a), and the global maximum voltage point (MVP), Figure 18(b), by the proposed approach is depicted in Figure 18. During fast changes in solar irradiance, the current varies following the MCP in a considerable and precise way, while the voltage varies weakly but precisely.

4.4.2. *Tracking MPPT by Conventional and Proposed Algorithms under Fast-Changing of Atmospheric Conditions before 0.2 Seconds.* When there are rapid and abrupt variations in sun irradiance, as depicted in Figure 19, the P&O MPPT approach presents several transient regimes corresponding to each stage of variation in solar irradiance, which

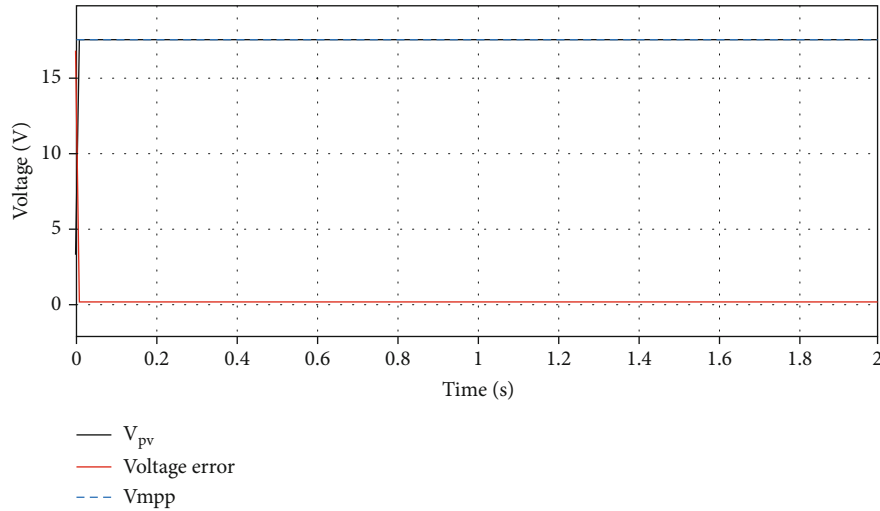
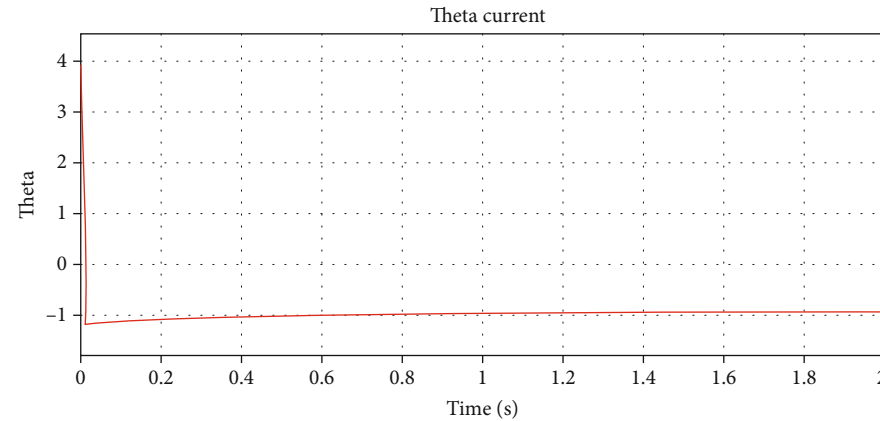
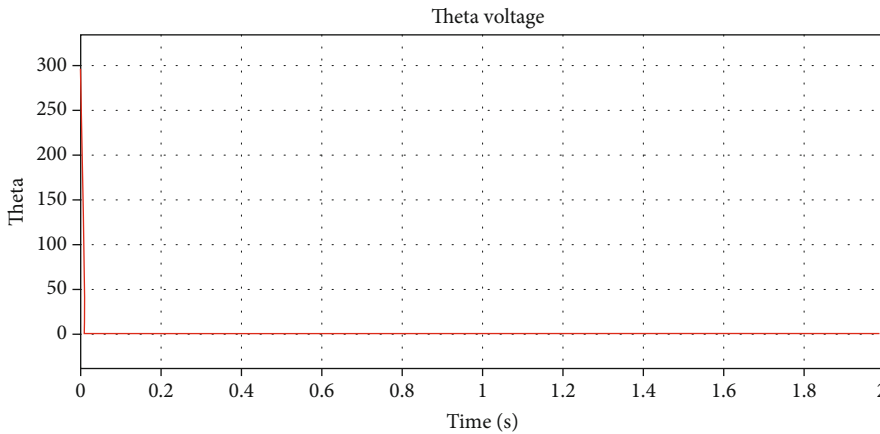


FIGURE 13: MRAC maximum voltage and error voltage point tracking in standard test conditions.



(a)



(b)

FIGURE 14: The current (a) and voltage (b) controller’s parameters of the MPPT MRAC array.

proves its difficulty in following a maximum power point in the case of fast and abrupt variations in sun irradiation, thus decreasing its efficiency in following the maximum power point under such atmospheric conditions. The INC and VSINC MPPT algorithms track a maximum power point

under sudden and rapid changes in solar irradiance, presenting for each of these two MPPT algorithms steady-state power fluctuations and overshoots that considerably affect their performance over the whole photovoltaic system under these atmospheric conditions.

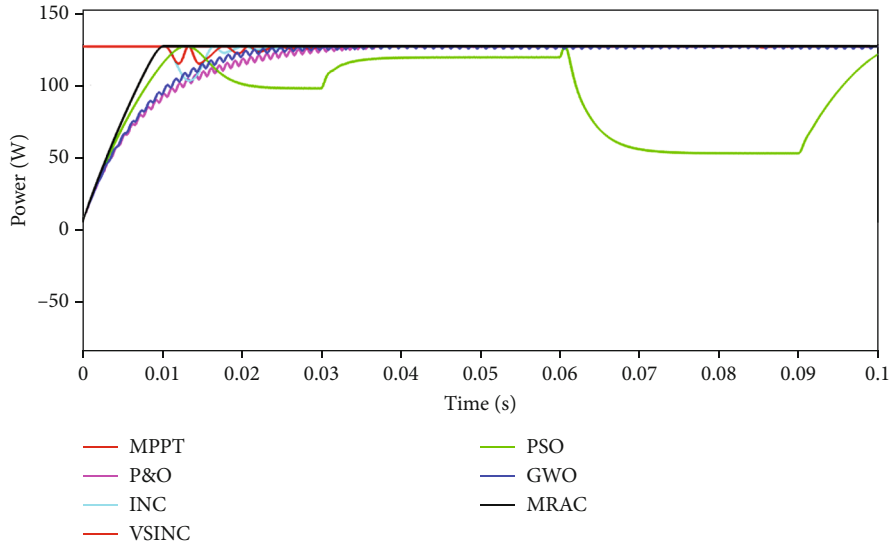


FIGURE 15: PV array power output tracking of P&O, INC, VSINC, PSO, GWO, and MRAC MPPT algorithms before 0.1 seconds in standard test conditions.

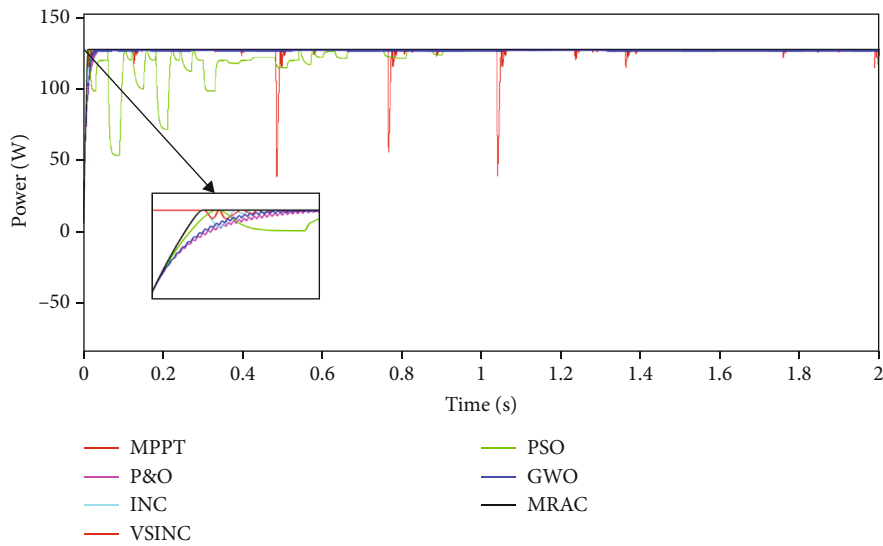


FIGURE 16: PV array power output tracking of the P&O, INC, VSINC, PSO, GWO, and MRAC MPPT algorithms before 0.2 seconds in standard test conditions.

4.4.3. *Dynamic and Static Performances of the Proposed and Standard MPPT Algorithms before 0.2 Seconds under Fast Changing Atmospheric Conditions.* The efficiency of the MPPT different algorithm denoted by η can be calculated as follows:

$$\eta = \frac{\int_0^2 P(t) dt}{\int_0^2 P_{\max}(t) dt} \times 100. \quad (53)$$

Table 4 shows the quantitative dynamic performance of the P&O, INC, VSINC, PSO, GWO, and MRAC MPPT algorithms. We can observe through Table 4 that the proposed MPPT MRAC approach not only improves but also

corrects the MPPT P&O, INC, VSINC, PSO, and GWO MPPT methods in terms of efficiency which is 99.09% for the P&O MPPT algorithm, 98.69% for the INC MPPT algorithm, 99.71% for the VSINC MPPT algorithm, 99.54% for the PSO MPPT algorithm, 98.97% for the GWO MPPT algorithm, and 99.88% for the MRAC MPPT algorithm. The convergence speed of the P&O, INC, VSINC, PSO, GWO, and MRAC MPPT approaches is reduced under rapid variations of atmospheric conditions than under normal conditions.

Table 5 shows the qualitative dynamic performance of P&O, INC, VSINC, PSO, GWO, and MRAC MPPT methods. We can observe through Table 5 that although all these algorithms guarantee the convergence of an MPP,

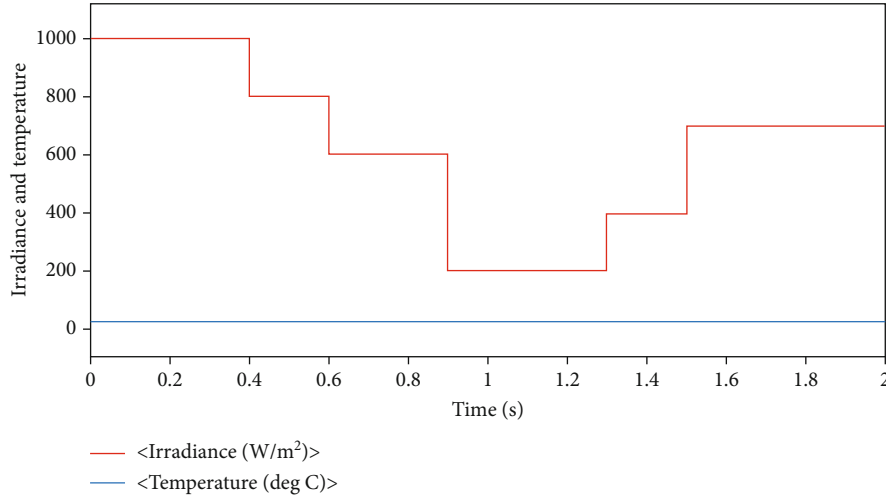


FIGURE 17: Profile of fast-changing of irradiance and fixed temperature 25°C for the test.

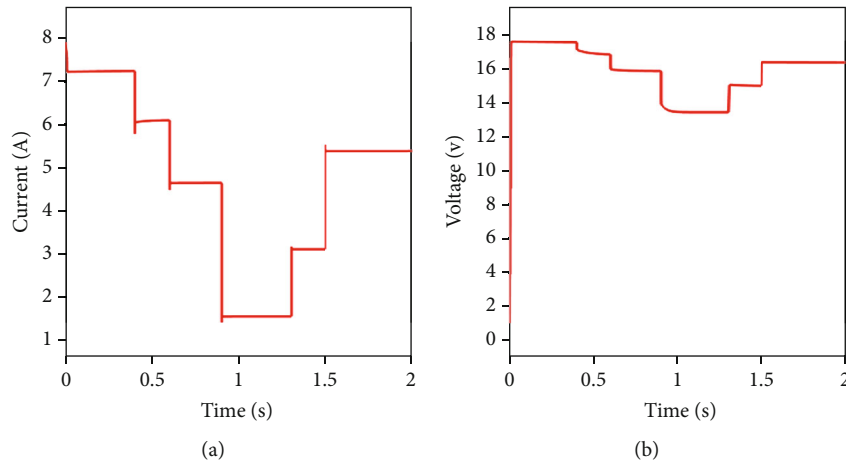


FIGURE 18: Tracking of a maximum current point (a) and a maximum voltage point (b) by the proposed approach under fast-changing atmospheric conditions.

the proposed MRAC MPPT approach corrects the other MPPT methods in terms of response time, oscillation around the MPP, power fluctuations, overshoot, reaching the MPP during rapid irradiation variations, robustness, etc. The proposed MPPT MRAC approach tracks very well the MPP; its complexity is medium; it is robust in the face of rapid variation in atmospheric conditions; and its accuracy to track the MPP is very high.

The static performances are illustrated in Figure 20; among these different algorithms, we observe that the MRAC MPPT approach suggested has the highest mean best value of 130 W, which compared to the mean best value indicates the best average compared to the other MPPT algorithms which are 129.6 W, 129.9 W, 125.5 W, 125.1 W, and 129.3 W, respectively, for P&O, INC, VSINC, PSO, and GWO.

According to Figure 20, the proposed MPPT approach presents a peak-to-peak power value of 129.2 W compared to the other methods, proving the best time response and the absence of overshoot and fluctuations in the power

under the curve obtained by the suggested MRAC MPPT approach.

The suggested MPPT approach according to Figure 20 has a root mean square (RMS) of 130.1 W at the highest and near the maximum power point, compared to the root mean square of the MPPT of the other MPPT algorithms, respectively, 129.7 W, 130 W, 126.6 W, 125.7 W, and 129.4 W, respectively, P&O, INC, VSINC, PSO, and GWO MPPT algorithms, proof that the proposed MRAC MPPT approach corrects the other algorithms in terms of power fluctuations and overshoot power.

The proposed MRAC MPPT algorithm according to Figure 20 shows that the maximum power of each algorithm is approximately equal to and near the maximum power point of the solar-powered cell, proving that all MPPT algorithms can follow the maximum power point at each, respectively, time response.

4.5. Discussion. By observing Figures 11 and 12, respectively, the error between the reference current and PV current

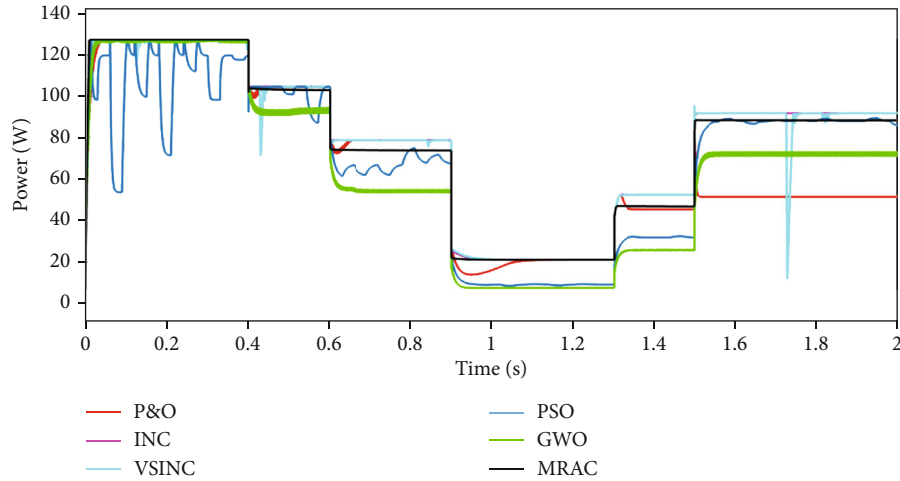


FIGURE 19: PV array power output tracking of P&O, INC, VSINC, PSO, GWO, and MRAC MPPT algorithms before 02 seconds under fast-changing atmospheric conditions.

TABLE 4: Dynamic quantitative comparative analysis of the different MPPT control algorithms.

Criteria for evaluation	P&O [23]	INC [27]	VSINC [39]	PSO [48]	GWO [49]	MRAC
Response time under normal test conditions	0.05 s	0.02 s	0.03 s	0.1 s	0.04 s	0.01 s
Response time under rapidly changing atmospheric conditions	0.04 s	0.01 s	0.02 s	0.09 s	0.03 s	0.009 s
Maximum PV voltage	17.76 V	17.37 V	17.65 V	17.52 V	16.87 V	17.58 V
Maximum PV current	07.33 A	07.48 A	07.38 A	07.43 A	07.451 A	07.41 A
Maximum PV power	130.3 W	130 W	130.3 W	130.3 W	130.3 W	130.3 W
Efficiency (%)	99.09	98.69	99.71	99.54	98.97	99.88

TABLE 5: Dynamic qualitative comparative analysis of the different MPPT algorithms.

Criteria for evaluation	P&O [23]	INC [27]	VSINC [39]	PSO [48]	GWO [49]	MRAC
MPP convergence	Guarantee	Guarantee	Guarantee	Guarantee	Guarantee	Guarantee
Ability to achieve MPP in CST	Yes	Yes	Yes	Yes	Yes	Yes
Ability to achieve MPP during atmospheric changes	Low	High	High	High	High	Very high
Ability to achieve GMPP	No	Yes	Yes	Yes	Yes	Yes
Complexity	Low	Medium	Medium	High	High	Medium
Power oscillations	High	Low	High	Low	Low	No
Robustness	No	Yes	Yes	Yes	Yes	Yes
Speed of convergence	Low	Medium	Fast	Fast	Fast	Very fast
Flexibility	Yes	Yes	Yes	Yes	Yes	Yes
Accuracy	Low	High	High	High	High	Very high

converges to 0, respectively, and the error between the PV voltage and the reference voltage also converges to zero with no oscillations. This proves the accuracy of the MRAC MPPT approach to follow the MPP current and voltage with no oscillations.

Before 0.1 seconds in standard test conditions where $G = 1000 \text{ W/m}^2$ and $T = 25^\circ\text{C}$, because we do not observe according to Figure 14, no steady-state oscillations and steady-state overshoot at 0.01s on the curve representing the suggested MRAC control approach, but the other MPPT algorithms approaches continue to oscillate considerably and the observations were done on the curves representing

the other algorithms conclude that, the proposed MRAC approach shows a best efficiency than GWO MPPT method by way of power oscillations around the MPP, shows best performances than the PSO MPPT algorithm in terms of MPP tracking and shows the best performance than the P&O, INC, VSINC, and GWO MPPT algorithms in terms of reducing the time in convergence to follow the MPP system in the steady-state. All this implies that the proposed MRAC MPPT control algorithm loses very little energy compared to other MPPT control algorithms before 0.1 s in standard test conditions. Apart from the PSO MPPT algorithm, which is remaining unstable, the P&O, INC, VSINC,

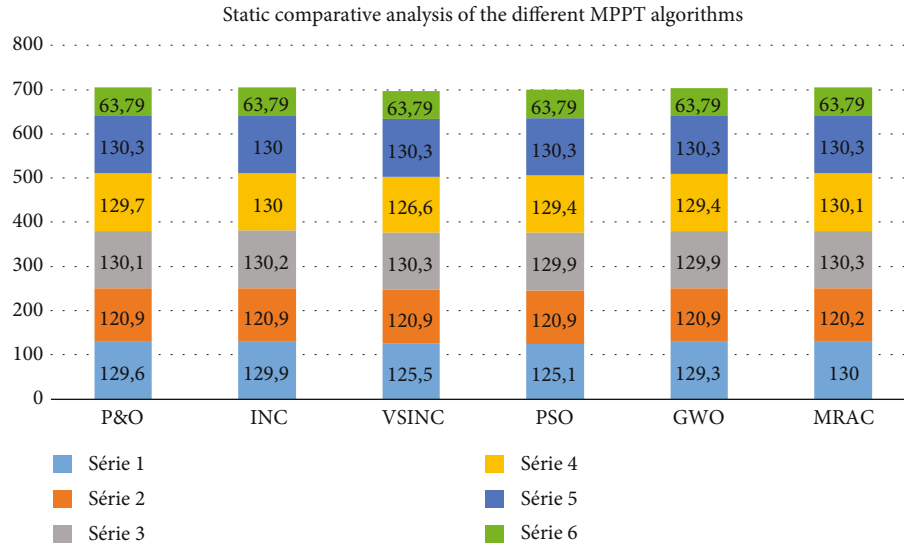


FIGURE 20: Static comparative analysis of P&O, INC, VSINC, PSO, GWO, and MRAC MPPT algorithms.

GWO, and MRAC MPPT algorithms, respectively, follow a maximum power point (130 W) following a time response of 0.05 s, 0.02 s, 0.03 s, 0.04 s, and 0.01 s for each algorithm.

However, in each tracking of a maximum power point, according to Figure 15, the VSINC MPPT algorithm curve shows the overshoot steady-state power, causing power losses and chattering effects and decreasing the performance of the PV system. Observations are made on steady-state power fluctuations observed by the GWO method. The PSO MPPT algorithm has big difficulty to track a maximum power point in its long and unstable transient regime, but in a steady-state system, it tracks a maximum power point perfectly following a time response of $t = 0.9$ s. This long tracking time of the maximum power point of the PSO MPPT method is likely affecting and significantly reducing the performance of the PV system caused by the complexity of this method. Observations are also made on the P&O and INC MPPT algorithms, which, although their response time is nevertheless lower than that of the VSINC, PSO, GWO, and MPPT methods, struggle in transient to follow a maximum power point, unlike the suggested MRAC MPPT approach which tracks a maximum power point perfectly with a very fast convergence rate. The absence of power fluctuations, overshoot, stability, robustness, and quick response time of the suggested MRAC approach will considerably increase the performance of the PV system as opposed to other MPPT algorithms. Under standard test conditions, before 02 seconds, these different MPPT methods are reliable and precise; the P&O method converges to a maximum power point (MPP) at 0.05 s and reaches a maximum power point of 130.3 W, the INC method converges to MPP at 0.02 s and reaches a maximum power of 130 W, the VSINC method converges to the MPP at 0.03 s and reaches a maximum power of 130.3 W, the PSO method converges to an MPP at 0.1 s and reaches a maximum power of 130.3 W, and the GWO control converges to the MPP at 0.04 s and reaches a maximum power of 130.3 W. Among these six

methods, the proposed MRAC control is the fastest with a response time of 0.01 s and reaches a maximum power of 130.3 W. The PSO control is the slowest and requires a tracking response time compared to the MRAC control, multiplied by 10 of 0.1 s. The proposed MRAC control reduces the response time; eliminates power fluctuations, power oscillations around the MPP, and power peaks; eliminates overshoot; and eliminates the steady-state chattering effect exhibited by P&O, INC, VSINC, PSO, and GWO methods, allowing the PV system to exhibit not only very critically damped but also optimal theoretical current, voltage, and power behavior. This shows how accurate the MRAC approach is and its capacity to determine the ideal duty cycle that will which deliver the greatest power at a steady state.

At rapid and abrupt variations of solar irradiance, according to Figure 19, the PSO MPPT algorithm in a transient regime has difficulty following the maximum power point because of its instability, but in a steady-state regime, this PSO MPPT algorithm follows the power point in its vicinity, for example, the maximum power of the MPPT PSO algorithm which is at 10 W, respectively, 30 W in the time interval $t = [0.9 \text{ s}; 1.3 \text{ s}]$ corresponding to the 200 W/m^2 irradiation, respectively, at $t = [1.3 \text{ s}; 1.5 \text{ s}]$ corresponding to the 400 W/m^2 irradiation, whereas the maximum power point is 20 W at the interval time $t = [0.9 \text{ s}; 1.3 \text{ s}]$ and 40 W, respectively, at $t = [1.3 \text{ s}; 1.5 \text{ s}]$. However, in the time interval $t = [1.5 \text{ s}; 2 \text{ s}]$ corresponding to the 700 W/m^2 irradiation at 80 W of MPPT, this PSO MPPT algorithm perfectly follows a maximum power point. At the same conditions of rapid and abrupt variations in solar irradiance, the GWO MPPT algorithm also follows the maximum power point in its vicinity, but also with power fluctuations. This is the case of the maximum power point of the MPPT GWO method, which is 90 W, respectively, 50 W, respectively, 10 W respectively, 20 W, respectively, and 60 W in the time interval $t = [0.4 \text{ s}; 0.6 \text{ s}]$ corresponding to the

800 W/m² irradiation, respectively, at $t = [0.6 \text{ s}; 0.9 \text{ s}]$ corresponding to the 600 W/m² irradiation, respectively, at $t = [0.9 \text{ s}; 1.3 \text{ s}]$ corresponding to the 200 W/m² irradiation, respectively, at $t = [1.3 \text{ s}; 1.5 \text{ s}]$ corresponding to the 400 W/m² irradiation and, respectively, at $t = [1.5 \text{ s}; 2 \text{ s}]$ corresponding to the 700 W/m² irradiation, respectively, while the maximum power point is 100 W at the interval time $t = [0.4 \text{ s}; 0.6 \text{ s}]$, at 60 W, respectively, at $t = [0.6 \text{ s}; 0.9 \text{ s}]$, at 30 W, respectively, at $t = [0.9 \text{ s}; 1.3 \text{ s}]$, at 50 W, respectively, at $t = [1.3 \text{ s}; 1.5 \text{ s}]$ and at 90 W, respectively, at $t = [1.5 \text{ s}; 2 \text{ s}]$. The PSO and GWO MPPT algorithms thus present, by following these observations, a loss of about 25% minimum energy at each stage of the irradiance of the sun that changes over time on the maximum power point to be reached at these different stages of variation of the solar irradiance. However, we observe that the GWO MPPT algorithm before the solar irradiance variation reaches the maximum power point, but with power fluctuations. Still, in solar irradiance variation, we also observe that the proposed MRAC MPPT approach follows considerably the maximum power point at different variation levels of irradiance, as observed in Figure 2(b) representing the P-V characteristics without overshoot and steady-state power fluctuations, being a stable, robust, and faster way than the other algorithms. The fluctuations and overshoots implied that there is an underdamped transient response in the system. With the MRAC MPPT approach, the underdamped mode power conversion can be eliminated and is robust, with the ability to avoid any transient oscillations. Thus, a shift in solar insolation is one example in which the PV system must be used. However, even after a shift in sunlight, the MRAC MPPT approach in Figure 19 displays no oscillatory response during all 02 s. Eliminating any potential underdamped response by the PV system owing to abrupt variations in solar insolation is one of the objectives of this study.

When there is fast variation in solar irradiation, the P&O algorithm converges to the MPP with a response time of 0.4 s, the INC algorithm converges to the MPP with a response time of 0.01 s, the VSINC algorithm converges to the MPP with a 0.02 s response time, the PSO algorithm converges to the MPP with a 0.9 s response time, the GWO algorithm converges to the MPP with a response time of 0.03 s, and the MRAC algorithm converges to the MPP with a 0.009 s response time.

Therefore, the suggested MRAC MPPT approach shows better performance than the P&O and VSINC MPPT methods by way of convergence speed, overshoot, steady-state power fluctuations, and oscillation around MPP, and the INC, PSO, and GWO MPPT algorithms in terms of the rate of reaching MPP and the initial convergence speed when the solar irradiance changes quickly. The INC, VSINC, PSO, and GWO MPPT methods can track MPP during very rapid and large changes in solar irradiance. The simulation results shown in Figure 19 show the effectiveness of following the MPP under very fast-changing atmospheric conditions with the proposed steady-state algorithm; there is no MPP ripple or oscillation, no overshoots, reduced response time, and elimination of the chattering phenomenon as opposed to P&O, INC, VSINC, PSO, and GWO MPPT algorithms.

5. Conclusion

This study presents a PV system with a boost converter integrated and coupled to a resistive load. Model reference adaptive control is used as the MPPT approach for the PV array under fast-changing atmospheric conditions. The tests were run in MATLAB/Simulink environment software under fast-changing atmospheric conditions and opposed to the output results of the P&O, INC, VSINC, PSO, and GWO methods. The simulation outcomes show that the suggested MRAC algorithm performs better than the standard PSO MPPT method in terms of stability and accuracy to reach the MPP, P&O, INC, VSINC, and GWO methods in terms of convergence speed, accuracy, ripple, and overshoot before 0.1 s in standard condition. The simulation also shows that the suggested MRAC algorithm outperforms the standard P&O, INC, VSINC, PSO, and GWO MPPT in terms of convergence speed, accuracy, ripple, overshoot, chattering effect, and efficiency before 2 s, both in standard and fast-changing atmospheric conditions. The proposed MRAC algorithm's robustness was given. The main limits remain the complexity of implementation of our proposed algorithm which is more of one of the P&O and INC methods, and the convergence speed obtained in fast-changing atmospheric conditions although low compared to the others is still high. Future article work will incorporate the proposed MRAC approach in real-time experimentally in the Arduino platform.

Acronyms

PV:	Photovoltaic
MPPT:	Maximum power point tracking
PVG:	Photovoltaic generator
MRAC:	Model reference adaptive control
P&O:	Perturb and observe
INC:	Incremental conductance
MPP:	Maximum power point
MCP:	Maximum current power
MVP:	Maximum voltage power
DC:	Direct current
VSINC:	Variable step incremental conductance
PSO:	Particle swarm optimization
GWO:	Grey wolf optimization.

Abbreviations

q :	The elementary electric charge ($1.6 \times 10^{-19} \text{ C}$)
K :	Boltzmann's constant (1.38×10^{-23})
V :	The voltage at the cell's terminals of v
n :	Ideality's factor ($1 < n < 3$)
T :	Ambient temperature ($^{\circ}\text{C}$)
n_s :	Number of series connected cells
n_p :	The number of parallel connected cells
I_0 :	The inverse saturation current (A)
I_{ph} :	The phase current flowing through a PV cell (A)
P_{max} :	Maximum power (w)
V_{MPP} :	Optimal voltage (v)
I_{MPP} :	Optimal current (A)

V_{oc} : Open circuit voltage (v)
 I_{sc} : Short circuit current (A)
 G : Solar irradiation (w/m^2)
 T : Junction temperature ($^{\circ}\text{C}$)
 R_s : Series resistor (Ω)
 R_{sh} : Shunt resistor (Ω)
 V_{pv} : Photovoltaic generator's voltage (v)
 P_{pv} : photovoltaic generator's power (w)
 I_{pv} : Current delivered by the photovoltaic generator (A).

Data Availability

No underlying data was collected or produced in this study.

Conflicts of Interest

There is no competing interest for all authors of this manuscript research.

Authors' Contributions

Y.A.M. was assigned to the conceptualisation of the project, writing, data retention, and formal analysis. J.K., J.V., U.N., M.D.D., and R.M. were responsible for the methodology, review, editing, and validation.

Acknowledgments

Our sincere thanks are due to the director, the head of the Department of Energy, Water and Environment laboratory, to the person in charge, to all teachers, and to the Ph.D students of the small hydro laboratory of the National Advanced School of Engineering of Yaounde, University of Yaounde1, Cameroon, who allowed the facilitation of our research.

References

- [1] U. Nzotcha, J. Kenfack, and M. B. Manjia, "Integrated multi-criteria decision making methodology for pumped hydro-energy storage plant site selection from a sustainable development perspective with an application," *Renewable and Sustainable Energy Reviews*, vol. 112, pp. 930–947, 2019.
- [2] AEI, "World energy investment outlook|special report," in The International Energy Agency (IEA), 2016.
- [3] J. Kenfack, O. V. Bossou, J. Voufo, S. Djom, and N. Crettenand, "New renewable energy promotion approach for rural electrification in Cameroon," in *Renewable Energy in the Service of Mankind Vol II*, pp. 429–442, Springer, Cham, 2016.
- [4] J. Kenfack, O. V. Bossou, J. Voufo, and S. Djom, "Addressing the current remote area electrification problems with solar and microhydro systems in Central Africa," *Renewable Energy*, vol. 67, pp. 10–19, 2014.
- [5] M. Vitale and D. Piazza, *Photovoltaic sources: modeling and emulation*, Springer, Verlag London, 2013.
- [6] M. M. Hassan, K. H. Refat, M. Z. Baten, and R. N. Sajjad, "Energy saving potential of photovoltaic windows: impact of shading, geography and climate," *Solar Energy*, vol. 240, pp. 342–353, 2022.
- [7] I. Tyukhov, "Advanced solar energy and educational technology," *Global Journal on Technology & Optimization*, vol. 1, pp. 2–9, 2010.
- [8] F. Xu, K. Gong, D. Liu, L. Wang, W. Li, and X. Zhou, "Enhancing photocurrent of dye-sensitized solar cells through solvent modulating aggregation of dyes," *Solar Energy*, vol. 240, pp. 157–167, 2022.
- [9] I. Sosa-Tinoco, M. A. Prósper, and G. Miguez-Macho, "Development of a solar energy forecasting system for two real solar plants based on WRF Solar with aerosol input and a solar plant model," *Solar Energy*, vol. 240, pp. 329–341, 2022.
- [10] A. Mohapatra, B. Nayak, P. Das, and K. B. Mohanty, "A review on MPPT techniques of PV system under partial shading condition," *Renewable and Sustainable Energy Reviews*, vol. 80, pp. 854–867, 2017.
- [11] A. R. Reisi, M. H. Moradi, and S. Jamsab, "Classification and comparison of maximum power point tracking techniques for photovoltaic system: a review," *Renewable and Sustainable Energy Reviews*, vol. 19, pp. 433–443, 2013.
- [12] B. Subudhi and R. Pradhan, "A comparative study on maximum power point tracking techniques for photovoltaic power systems," *IEEE Transactions on Sustainable Energy*, vol. 4, no. 1, pp. 89–98, 2013.
- [13] L. Gil-Antonio, M. B. Saldivar-Marquez, and O. Portillo-Rodriguez, "Maximum power point tracking techniques in photovoltaic systems: a brief review," in *2016 13th International Conference on Power Electronics (CIEP)*, pp. 317–322, Guanajuato, Mexico, 2016.
- [14] M. A. Enany, M. A. Farahat, and A. Nasr, "Modeling and evaluation of main maximum power point tracking algorithms for photovoltaics systems," *Renewable and Sustainable Energy Reviews*, vol. 58, pp. 1578–1586, 2016.
- [15] S. Dorahaki, "Evaluating the radiation and temperature effect on photovoltaic systems," *Bulletin of Electrical Engineering and Informatics*, vol. 4, no. 1, pp. 1–6, 2015.
- [16] R. Prasanth and K. Young-Jin, "A simple, reliable and adaptive approach to estimate photovoltaic parameters using spotted hyena optimization: A framework intelligent to predict photovoltaic parameters for any meteorological change," *Solar Energy*, vol. 236, pp. 480–498, 2022.
- [17] J. Ahmed and Z. Salam, "A modified P&O maximum power point tracking method with reduced steady-state oscillation and improved tracking efficiency," *IEEE Transactions on Sustainable Energy*, vol. 7, no. 4, pp. 1506–1515, 2016.
- [18] T. Noguchi, S. Togashi, and R. Nakamoto, "Short-current pulse-based maximum-power-point tracking method for multiple photovoltaic-and-converter module system," *IEEE Transactions on Industrial Electronics*, vol. 49, no. 1, pp. 217–223, 2002.
- [19] K. Kobayashi, H. Matsuo, and Y. Sekine, "A novel optimum operating point tracker of the solar cell power supply system," in *2004 IEEE 35th Annual Power Electronics Specialists Conference (IEEE Cat. No.04CH37551)*, pp. 2147–2151, Aachen, Germany, 2004.
- [20] A. K. Abdelsalam, A. M. Massoud, S. Ahmed, and P. N. Enjeti, "High-performance adaptive perturb and observe MPPT technique for photovoltaic-based microgrids," *IEEE Transactions on Power Electronics*, vol. 26, no. 4, pp. 1010–1021, 2011.
- [21] N. Kumar, B. Singh, and B. K. Panigrahi, "ANOVA Kernel Kalman filter for multi-objective grid integrated solar photovoltaic-distribution static compensator," *IEEE Transactions on Circuits*

- and Systems I: Regular Papers, vol. 66, no. 11, pp. 4256–4264, 2019.
- [22] B. Singh, N. Kumar, and B. K. Panigrahi, “Steepest descent Laplacian regression based neural network approach for optimal operation of grid supportive solar PV generation,” *IEEE Transactions on Circuits and Systems II: Express Briefs*, vol. 68, no. 6, pp. 1947–1951, 2021.
 - [23] F. U. Nazir, N. Kumar, B. C. Pal, B. Singh, and B. K. Panigrahi, “Enhanced SOGI controller for weak grid integrated solar PV system,” *IEEE Transactions on Energy Conversion*, vol. 35, no. 3, pp. 1208–1217, 2020.
 - [24] T. Eram and P. L. Chapman, “Comparison of photovoltaic array maximum power point tracking techniques,” *IEEE Transactions on Energy Conversion*, vol. 22, pp. 439–449, 2007.
 - [25] V. Salas, E. Olias, A. Barrado, and A. Lázaro, “Review of the maximum power point tracking algorithms for stand-alone photovoltaic systems,” *Solar Energy and Solar Cells*, vol. 90, pp. 1555–1578, 2006.
 - [26] N. Kumar, B. Singh, and B. K. Panigrahi, “Framework of gradient descent least squares regression based-NN structure for power quality improvement in PV-integrated low-voltage weak grid system,” *IEEE Transactions on Industrial Electronics*, vol. 66, no. 12, pp. 9724–9733, 2019.
 - [27] A. Safari and S. Mekhilef, “Simulation and hardware implementation of incremental conductance MPPT with direct control method using Cuk converter,” *IEEE Transactions on Industrial Electronics*, vol. 58, no. 4, pp. 1154–1161, 2011.
 - [28] R. Mohamed, M. Ebrahim, F. Bendary, and S. Osman, “Transient stability enhancement for 20 MW PV power plant via incremental conductance controller,” *International Journal of System Dynamics Applications*, vol. 6, no. 4, pp. 102–123, 2017.
 - [29] S. Sajadian, R. Ahmadi, and H. Zargarzadeh, “Extremum seeking-based model predictive MPPT for grid-tied Z-source inverter for photovoltaic systems,” *IEEE Journal of Emerging and Selected Topics in Power Electronics*, vol. 7, pp. 226–227, 2019.
 - [30] A. Mehiri, M. Bettayeb, A. K. Hamid, and A. Ardjal, “Fractional nonlinear synergetic control for DC-link voltage regulator of three phase inverter grid-tied PV system,” in *2018 5th International Conference on Renewable Energy: Generation and Applications (ICREGA)*, pp. 90–93, Al Ain, United Arab Emirates, 2018.
 - [31] V. M. Lucia, L. A. Maria, D. N. Mario, D. V. Paola, S. Allexandra, and P. Carlo, “Thin film silicon photovoltaics: architectural perspectives and technological issues,” *Applied Energy*, vol. 86, no. 10, pp. 1836–1844, 2009.
 - [32] F. T. Mabvuer, F. T. Nya, and G. M. Kenfack, “Improving the absorption spectrum and performance of CIGS solar cells by optimizing the stepped band gap profile of the multilayer absorber,” *Solar Energy*, vol. 240, pp. 193–200, 2022.
 - [33] R. Kotti and W. Shireen, “Efficient MPPT control for PV systems adaptive to fast changing irradiation and partial shading conditions,” *Solar Energy*, vol. 114, pp. 397–407, 2015.
 - [34] A. Gupta, Y. K. Chauhan, and R. K. Pachauri, “A comparative investigation of maximum power point tracking methods for solar PV system,” *Solar Energy*, vol. 136, pp. 236–253, 2016.
 - [35] A. Chalh, S. Motahhir, A. E. Ghzizal, A. E. Hammoumi, and A. Derouich, “Global MPPT of photovoltaic system based on scanning method under partial shading condition,” *SN Applied Sciences*, vol. 2, no. 4, p. 771, 2020.
 - [36] K. Nishant, S. Bhim, and K. P. Bijaya, “LLMLF-based control approach and LPO MPPT technique for improving performance of a multifunctional three-phase two-stage grid integrated PV system,” *IEEE Transactions on Sustainable Energy*, vol. 11, no. 1, pp. 371–380, 2019.
 - [37] N. Kumar, B. Singh, and B. K. Panigrahi, “Integration of solar PV with low-voltage weak grid system: using Maximize-M Kalman filter and self-tuned P&O algorithm,” *IEEE Transactions on Industrial Electronics*, vol. 66, no. 11, pp. 9013–9022, 2019.
 - [38] F. Liu, S. Duan, F. Liu, B. Liu, and Y. Kang, “A Variable Step Size INC MPPT Method for PV Systems,” *IEEE Transactions on Industrial Electronics*, vol. 55, no. 7, pp. 2622–2628, 2008.
 - [39] K. S. Tey and S. Mekhilef, “Modified incremental conductance MPPT algorithm to mitigate inaccurate responses under fast-changing solar irradiation level,” *Solar Energy*, vol. 101, pp. 333–342, 2014.
 - [40] N. Kumar, B. Singh, B. K. Panigrahi, and L. Xu, “Leaky-least-logarithmic-absolute-difference-based control algorithm and learning-based InC MPPT technique for grid-integrated PV system,” *IEEE Transactions on Industrial Electronics*, vol. 66, no. 11, pp. 9003–9012, 2019.
 - [41] N. Kumar, B. Singh, B. K. Panigrahi, C. Chakraborty, H. M. Suryawanshi, and V. Verma, “Integration of solar PV with low-voltage weak grid system: Using normalized laplacian kernel adaptive kalman filter and learning based InC algorithm,” *IEEE Transactions on Power Electronics*, vol. 34, no. 11, pp. 10746–10758, 2019.
 - [42] N. Kumar, B. Singh, J. Wang, and B. K. Panigrahi, “A framework of L-HC and AM-MKF for accurate harmonic supportive control schemes,” *IEEE Transactions on Circuits and Systems I: Regular Papers*, vol. 67, no. 12, pp. 5246–5256, 2020.
 - [43] K. Nishant, S. Bhim, and K. P. Bijaya, “PNKLMF-based neural network control and learning-based HC MPPT technique for multiobjective grid integrated solar PV based distributed generating system,” *IEEE Transactions on Industrial Informatics*, vol. 15, no. 6, pp. 3732–3742, 2019.
 - [44] S. Immad, M. Saad, and S. T. Kok, “Maximum power point tracking using modified butterfly optimization algorithm for partial shading, uniform shading, and fast varying load conditions,” *Transactions on Power Electronics*, vol. 36, pp. 5569–5581, 2021.
 - [45] S. T. Kok, M. Saad, S. Mehdi, and B. Horan, “Improved differential evolution-based MPPT algorithm using SEPIC for PV systems under partial shading conditions and load variation,” *IEEE Transactions on Industrial Informatics*, vol. 99, p. 1, 2018.
 - [46] L. Lian, R. Srivatsan, and L. Douglas, “Computational intelligence techniques for maximum power point tracking in PV systems: a review,” *Renewable and Sustainable Energy Reviews*, vol. 85, pp. 14–45, 2018.
 - [47] R. Boukenoui, H. Salhi, R. Bradai, and A. Mellit, “A new intelligent MPPT method for stand-alone photovoltaic systems operating under fast transient variations of shading patterns,” *Solar Energy*, vol. 124, pp. 124–142, 2016.
 - [48] D. M. Djanssou, A. Dadjé, A. Tom, and N. Djongyang, “Improvement of the dynamic response of robust sliding mode MPPT controller-based PSO algorithm for PV systems under fast-changing atmospheric conditions,” *International Journal of Photoenergy*, vol. 2021, Article ID 6671133, 3 pages, 2021.
 - [49] M. Satyajit, S. Bidyadhar, and P. R. Kumar, “A new MPPT design using grey wolf optimization technique for photovoltaic

- system under partial shading conditions,” *IEEE Trans on Sustainable Energy*, vol. 7, no. 1, pp. 181–188, 2016.
- [50] B. Peng, K. Ho, and Y. Liu, “A novel and fast MPPT method suitable for both fast changing and partially shaded conditions,” *IEEE Transaction on Industrial Electronics*, vol. 65, no. 4, pp. 3240–3251, 2018.
- [51] K. Sundareswaran, S. Peddapati, and S. Palani, “MPPT of PV systems under partial shaded conditions through a colony of flashing fireflies,” *IEEE Transaction on Energy Conversion*, vol. 29, no. 2, pp. 463–472, 2014.
- [52] C. Huang, L. Wang, R. S. Yeung, Z. Zhang, H. S. Chung, and A. Bensoussan, “A prediction model-guided Jaya algorithm for the PV system maximum power point tracking,” *IEEE Transaction on Sustainable Energy*, vol. 9, no. 1, pp. 45–55, 2018.
- [53] T. Kok Soon, M. Saad, Y. Hong-Tzer, and C. Ming-Kai, “A differential evolution based MPPT method for photovoltaic modules under partial shading conditions,” *International Journal of Photoenergy*, vol. 2014, Article ID 945906, 10 pages, 2014.
- [54] D. Fares, M. Fathi, I. Shams, and S. Mekhilef, “A novel global MPPT technique based on squirrel search algorithm for PV module under partial shading conditions,” *Energy Conversion and Management*, vol. 230, article 113773, 2021.
- [55] A. Badis, M. Mansouri, and M. Boujmil, “A genetic algorithm optimized MPPT controller for a PV system with DC-DC boost converter,” in *2017 International Conference on Engineering & MIS (ICEMIS)*, pp. 1–6, Monastir, Tunisia, 2017.
- [56] A. Benyoucefa, A. Chouderb, K. Karaa, S. Silvestrec, and O. Sahedaa, “Artificial bee colony based algorithm for maximum power point tracking (MPPT) for PV systems operating under partial shaded conditions,” *Applied Soft Computing*, vol. 32, pp. 38–48, 2015.
- [57] R. Santi Agatino and S. Giacomo, “ANN based MPPT method for rapidly variable shading conditions,” *Applied Energy*, vol. 145, pp. 124–132, 2015.
- [58] K. Ahmad, A. Nasrudin, S. Jeyraj, and M. Nasir Uddin, “Fuzzy-Logic-Controller-Based SEPIC converter for maximum power point tracking,” *IEEE Transaction on Industrial Applied*, vol. 50, no. 4, pp. 2349–2358, 2014.
- [59] M. Kermadi and E. Berkouk, “Artificial intelligence-based maximum power point tracking controllers for photovoltaic systems: comparative study,” *Renewable and Sustainable Energy Reviews*, vol. 69, pp. 369–386, 2017.
- [60] W. Bin, “Adaptive control design and stability analysis of robotic manipulators,” *Actuators*, vol. 7, no. 4, p. 89, 2018.
- [61] R. Khanna, Q. Zhang, W. E. Stanchina, G. F. Reed, and Z. H. Mao, “Maximum power point tracking using model reference adaptive control,” *IEEE Transactions on Power Electronics*, vol. 29, no. 3, pp. 1490–1499, 2014.
- [62] T. Matsui, H. Sai, A. Bidiville, H. J. Hsu, and K. Matsubara, “Progress and limitations of thin-film silicon solar cells,” *Solar Energy*, vol. 170, pp. 486–498, 2018.
- [63] C. Y. Tsai and C. Y. Tsai, “Tandem amorphous/microcrystalline silicon thin-film solar modules: developments of novel technologies,” *Solar Energy*, vol. 170, pp. 419–429, 2018.
- [64] O. Isabella, R. Vismara, D. N. Linssen, K. X. Wang, S. Fan, and M. Zeman, “Advanced light trapping scheme in decoupled front and rear textured thin-film silicon solar cells,” *Solar Energy*, vol. 162, pp. 344–356, 2018.
- [65] J. Bikaneria, S. P. Joshi, and A. R. Joshi, “Modeling and simulation of PV cell using one-diode model,” *International Journal of Scientific and Research Publications*, vol. 3, no. 10, pp. 2250–3153, 2013.
- [66] D. Winston, B. Kumar, S. Christabel, A. Chamkha, and R. Sathyamurthy, “Maximum power extraction in solar renewable power system—a bypass diode scanning approach,” *Computers & Electrical Engineering*, vol. 70, pp. 122–136, 2018.
- [67] M. Libra, T. Petřík, V. Poulek, I. I. Tyukhov, and P. Kouřím, “Changes in the efficiency of photovoltaic energy conversion in temperature range with extreme limits,” *IEEE Journal of Photovoltaics*, vol. 11, no. 6, pp. 1479–1484, 2021.
- [68] R. F. Coelho, F. Concer, and D. C. Martins, “A study of the basic DC-DC converters applied in maximum power point tracking,” in *2009 Brazilian Power Electronics Conference*, pp. 673–678, Bonito-Mato Grosso do Sul, Brazil, 2009.
- [69] S. T. Kok, M. Saad, S. Mehdi, H. Ben, T. Amanullah, and S. Alex, “Improved differential evolution-based MPPT algorithm using SEPIC for PV systems under partial shading conditions and load variation,” *IEEE Transactions on Industrial Informatics*, vol. 14, no. 10, pp. 4322–4333, 2018.
- [70] T. Bennett, A. Zoulchian, and R. Messenger, “Photovoltaic model and converter topology considerations for MPPT purposes,” *Solar Energy*, vol. 86, no. 7, pp. 2029–2040, 2012.
- [71] D. E. Miller, “A new approach to model reference adaptive control,” *IEEE Transactions on Automatic Control*, vol. 48, no. 5, pp. 743–757, 2003.
- [72] S. Sastry and M. Bodson, *Adaptive Control: Stability, Convergence and Robustness*, Dover Publications, New York, NY, USA, 2011.
- [73] P. A. Ioannou and J. Sun, *Robust Adaptive Control*, Prentice Hall, Englewood Cliff, NJ, USA, 1996.
- [74] K. R. Meyer, “On the Existence of Lyapunov Function for the Problem of Lur’e,” *Journal of the Society for Industrial and Applied Mathematics, Series A: Control*, vol. 3, no. 3, pp. 373–383, 1965.
- [75] R. Chenni and R. Mehimmedetsi, “Modelling of DC PV system with MPPT,” in *2015 3rd International Renewable and Sustainable Energy Conference (IRSEC)*, pp. 1–6, Marrakech, Morocco, 2015.
- [76] S. R. Wenham, M. A. Green, M. E. Watt, and R. Corkish, *Applied Photovoltaics*, Earthscan, London, UK, 2nd edition, 2007.